Monthly Notices
of the
ROYAL ASTRONOMICAL SOCIETY

MNRAS **448,** 2245–2259 (2015) doi:10.1093/mnras/stv168

Complex narrow-line Seyfert 1s: high spin or high inclination?

Emma Gardner★ and Chris Done

Department of Physics, University of Durham, South Road, Durham DH1 3LE, UK

Accepted 2015 January 21. Received 2015 January 19; in original form 2014 November 21

ABSTRACT

Complex narrow-line Seyfert 1s (NLS1s), such as 1H 0707−495, differ from simple NLS1s like PG 1244+026 by showing stronger broad spectral features at Fe K and larger amplitude flux variability. These are correlated: the strongest Fe K features are seen during deep dips in the light curves of complex NLS1s. There are two competing explanations for these features, one where a compact X-ray source on the spin axis of a highly spinning black hole approaches the horizon and the consequent strong relativistic effects focus the intrinsic flux on to the inner edge of a thin disc, giving a dim, reflection-dominated spectrum. The other is that the deep dips are caused by complex absorption by clumps close to the hard X-ray source. The reflection-dominated model is able to reproduce the very short 30 s soft lag from reverberation seen in the complex NLS1 1H 0707−495. However, it does not explain the characteristic switch to hard lags on longer time-scales. Instead, a full model of propagating fluctuations coupled to reverberation can explain the switch in the simple NLS1 PG 1244+026 using a low spin black hole. However, PG 1244+026 has a longer reverberation lag of ∼200 s. Here we extend the successful propagation–reverberation model for the simple NLS1 PG 1244+026 to include the effect of absorption from clumps in a turbulent region above the disc. The resulting occultations of the inner accretion flow can introduce additional hard lags when relativistic effects are taken into account. This dilutes the soft lag from reverberation and shifts it to higher frequencies, making a smooth transition between the 200 s lags seen in simple NLS1s to the 30 s lags in complex NLS1s. These two classes of NLS1 could then be determined by inclination angle with respect to a clumpy, probably turbulent, failed wind structure on the disc.

Key words: accretion, accretion discs – black hole physics – galaxies: individual: PG 1244+026 – galaxies: individual: 1H 0707−495 – galaxies: Seyfert – X-rays: galaxies.

1 INTRODUCTION

Narrow-line Seyfert type 1s (NLS1s) are small mass, high mass accretion rate active galactic nuclei (AGN). Like other AGN, their fastest, highest amplitude variability is at X-ray energies, but their lower mass means that this variability is on shorter time-scales, making it easier to study over a typical <1 d observation (e.g. Ponti et al. 2010).

All the NLS1s show rapid X-ray variability (Leighly 1999), but some also show deep dips in the X-ray light curve. These dips coincide with the appearance of high energy complexity in the 2–10 keV spectra, either gradual curvature or strong features around the Fe Kα line energy. Gallo (2006) termed these 'complex' NLS1s to distinguish them from the 'simple' NLS1s which do not show dips and have relatively power-law-like spectra from 2 to 10 keV. Two different models have been proposed to explain the deep dips and associated spectral complexity: partial covering and relativistic reflection.

In the partial covering model, the dips are caused by low ionization material moving into the line of sight, increasing the absorption at the iron edge energy at 7.1 keV. This material can only partially cover the source as some fraction of the flux at low energies is still seen (e.g. Inoue & Matsumoto 2003; Turner et al. 2007; Miyakawa, Ebisawa & Inoue 2012). Conversely, in the relativistic reflection model the dips are caused by an extremely compact X-ray source on the spin axis of the black hole (BH) approaching the event horizon. The resulting strong light bending focuses the intrinsic continuum away from the observer (producing the drop in flux) so it instead strongly illuminates the very inner disc. For high spin BHs the resulting spectrum can be dominated by highly smeared relativistic reflection, marked by a strong but extremely broad and skewed Fe Kα line (e.g. Fabian et al. 2004, 2009; Miniutti & Fabian 2004). In both models, the 'complex' and 'simple' NLS1s are intrinsically similar, and can change from one to the other (as observed; Gallo 2006) depending on whether there is absorption along the line of

★ E-mail: e.l.gardner@dur.ac.uk

sight, or in the reflection model, whether the compact X-ray source is close to the horizon.

Both absorption and reflection models can fit the observed 0.3–10 keV spectra, as fitting complex models over a limited bandpass is highly degenerate. However, a recent breakthrough is in the use of variability to break some of these degeneracies. In particular, the new techniques which can identify a lagged signal are clearly well matched to the reflection models, where there is a strong prediction that the reflected emission should lag behind the intrinsic continuum variability on the light travel time (Fabian et al. 2009; Uttley et al. 2014). Detection of a very short lag time (∼30 s) in the complex NLS1 1H 0707−495 is taken as unequivocal support for the high spin relativistic reflection picture, as this implies distances of the source from the disc of $<2R_{\rm g}$ for a $3 \times 10^6\,{\rm M}_{\odot}$ BH. The 'simple' NLS1 PG 1244+026 shows a much longer lag time of ∼200 s (Alston, Done & Vaughan 2014), consistent with the source being somewhat further from the horizon.

Lags are derived by comparing variability in a soft and hard band, and show much more structure than just the reverberation signal. The lags change as a function of the time-scale of variability. The soft leads the hard for long time-scale variability, then this lag decreases with decreasing variability time-scale until it goes negative (soft lagging) for the fastest fluctuations. This characteristic soft lead decreasing with frequency was first seen in the (much higher signal-to-noise ratio) black hole binaries (BHBs; e.g. Miyamoto et al. 1988; Nowak et al. 1999), where it is now interpreted as the signature of fluctuations propagating through an inhomogeneous accretion flow (Kotov, Churazov & Gilfanov 2001; Arévalo & Uttley 2006). Slow variability starts at large radii, where the spectrum is softer. It then propagates down through the entire flow until it gets to the centre, modulating the hardest spectral region. Faster variability is only produced closer to the BH. It has a shorter distance to travel to reach the inner regions so takes a shorter time before it modulates the hardest X-ray component from the centre, i.e. this characteristic lag pattern is produced by a correlation of spectrum and variability with radial position. But this also means that the soft and hard bands both contain some emission from the softer spectrum produced at large radii, and the harder spectrum produced at smaller radii. There is just more of the softer (large radii) spectrum in the soft band than in the hard (and conversely, more of the harder, small radii spectrum in the hard band than in the soft). Thus each band contains the same components, but with different weighting, so most of the variability is perfectly correlated, with only a very small fraction which is lagged. This is seen in BHBs in a cross-correlation of hard and soft bands, which always peaks at zero lag, with just a small asymmetry (Torii et al. 2011). The important point for AGN is that the spectral content of the hard and soft bands matters, and that the lags are diluted if the same component appears in both bands (Miller et al. 2010; Uttley et al. 2014).

Thus lags between light curves in two different energy bands have to be interpreted with a model of the spectral components which contribute to each band. Even the 'simple' NLS1 PG 1244+026 has a spectrum which requires multiple components. These can either be modelled by a disc, low-temperature Comptonization and high-temperature Comptonization, together with its (weak and only weakly smeared) reflection from a disc, or with disc, high-temperature Comptonization and its (strong, and strongly smeared) reflection from a disc (Jin et al. 2013), or with a steep power law (presumably from the jet?) together with high-temperature Comptonization and its (strong and strongly smeared) reflection from a disc (Kara et al. 2014). Using variability breaks degeneracies, and the combined constraints from energy spectra, power spectra in hard and soft bands, high frequency covariance spectra from the 4 to 10 keV light curve (the spectrum of the fast variability which correlates with the 4–10 keV light curve) and the lag-frequency spectrum strongly support the first model. In this model, slow fluctuations in the disc propagate down to modulate faster variability in the soft excess (dominated by the low-temperature Compton emission), which propagates down into the high-temperature Compton emission from the X-ray corona, which then reflects from and is reprocessed by the disc. None of the models with strong, strongly smeared relativistic reflection could adequately match all the spectral timing data for this source (Gardner & Done 2014, hereafter GD14). In particular the fact relativistic reflection contributes strongly to both the hard and soft bands, results in nearly identical hard and soft band power spectra and high coherence between hard and soft bands up to high frequencies, in disagreement with observations of PG 1244+026.

This model had no constraints on spin, as the disc component came from 20 to $12R_{\rm g}$, the soft excess from 12 to $6R_{\rm g}$ and the coronal size was assumed to be $6R_{\rm g}$. The soft X-ray excess is a composite of a separate low-temperature Comptonization component from the disc (which carries the required propagation signal) and the mostly thermalized reprocessed emission from non-reflected X-ray illumination of the disc. Hence the soft band contains components which carry the soft lead and the soft lag, but identifying the lag with reprocessing rather than reflection removes the requirement for extreme relativistic smearing as the thermalized emission is already smooth, as seen in the data, quite unlike ionized reflection which has strong atomic features. *Nuclear Spectroscopic Telescope Array* (*NuSTAR*) data (Akn 120; Matt et al. 2014) and long-term X-ray/ultraviolet (UV) variability (Mrk 509; Mehdipour et al. 2011; Petrucci et al. 2013; Boissay et al. 2014) favour the low-temperature Comptonization model for the soft X-ray excess in standard broad-line Seyfert 1s. This removes the requirement of high spin derived from assuming that this component is instead from ionized reflection (Patrick et al. 2011; see also Crummy et al. 2006), but we note that the issue is still controversial, and probably complex (Lohfink et al. 2012).

With this model, the lag in PG 1244+026 does not require high spin but neither does it rule out a source at $\sim 6R_{\rm g}$ above the event horizon of a high spin BH, still allowing the range from 'simple' to 'complex' behaviour to be due to the height of the source. However, the broad-band spectral energy distribution *does* rule out a standard disc around a high spin BH. The observed optical/UV continuum constrains the mass accretion rate on to the BH given its mass, so the total luminosity is only dependent on the efficiency, i.e. on BH spin. A high spin BH produces too much luminosity which is very difficult to hide even in the UV–extreme ultraviolet (EUV) interstellar absorption gap (Done et al. 2013). Advection is unlikely to change this conclusion, first as this source is not strongly super-Eddington, and secondly as the most recent global radiative magnetorotational instability (MRI; but Newtonian) disc simulations of a super-Eddington flow at $\dot{M}_{\rm in} = 20\dot{M}_{\rm Edd}$ show that this is still almost as radiatively efficient as a standard thin disc due to vertical convection (Jiang, Stone & Davis 2014). Thus this source is most likely low spin, so should never show the extremely deep dips which are characteristic of the 'complex' NLS1, as a low spin BH cannot produce extreme light bending. This is because the steep emissivity index required can only be produced when the illuminating source height is $<2R_{\rm g}$ (Dovciak et al. 2014), which for a low spin BH is below the horizon. This suggests that 'simple' to 'complex' is more than just the source height, and points instead to

spin as the potential difference between the two classes. Yet many NLS1s show transitions between 'simple' and 'complex' behaviour (Gallo 2006; Miller, Turner & Reeves 2008) so spin cannot be the origin of the difference either.

The accretion flow in steady state should only depend on BH mass, spin and mass accretion rate, plus inclination with respect to the disc which can change its appearance. All the NLS1s have similar mass and mass accretion rate (within a factor of ∼3) so if the difference between 'simple' and 'complex' is neither source height nor spin, then inclination is the last parameter to try. These sources are all around Eddington, so it seems unlikely that they are actually described by a flat disc as assumed in the relativistic reverberation models. The global MRI simulation at $\dot{M}_{\rm in} = 20\dot{M}_{\rm Edd}$ showed a complex flow structure, with a large scale height radiation-pressure-driven wind from the inner disc carrying away 30 per cent of the input mass accretion rate (Jiang et al. 2014). This wind is likely to be less strong in PG 1244+026 since this source is only $\dot{M}_{\rm in} \sim \dot{M}_{\rm Edd}$. UV line driving is unlikely to help since the low mass and high mass accretion rate of NLS1s mean that their disc is too hot for its photosphere to have the required opacity to UV line transitions (Hagino et al. 2015).

Hence strong mass loss is not expected in the NLS1s, but some turbulent, clumpy, failed Eddington wind in the inner disc could easily form (Jiang et al. 2014). High inclination angles have a high probability of a clump intersecting the line of sight, while low inclination angles are mostly free of obscuration, giving a potential mapping from complex to simple NLS1 as a function of inclination. The spectral signature of this time-dependent absorption could be complex, depending on the amount of source occulted and the ionization state of the absorber.

Here we explore the effect of occultations on the lag-frequency behaviour. We show that occultations produce a soft lead when relativistic Doppler effects are taken into account. We couple orbiting clump occultations with the full spectral timing model developed in GD14 to explain the properties of the simple NLS1 PG 1244+026. We show that multiple occultations of this intrinsic propagation and reprocessing/reflection model can replicate the change in observed lag-frequency properties from a simple to a complex NLS1. In particular the soft lead resulting from occultations dilutes the maximum measured reverberation lag and shifts it to higher frequencies, as observed.

Many issues still remain for this to be a full model of the complex NLS1. Nevertheless, this shows a promising alternative geometry for the complex NLS1.

2 LINEAR OCCULTATION

We choose to model the underlying accretion flow using the separate soft excess model found by GD14 to describe the spectral timing properties of the simple NLS1 PG 1244+026. We assume the accretion flow consists of three components. The outermost radii form a standard accretion disc. This is truncated at some radius ($R_{\rm cor} \sim 20R_{\rm g}$). The remaining gravitational energy liberated between $R_{\rm cor}$ and the innermost stable circular orbit ($R_{\rm isco}$) is used to power the remaining two components: the soft excess and the corona. Below $R_{\rm cor}$ material is unable to thermalize completely and form a cool accretion disc, perhaps due to a larger scale height from the photosphere lifting to form the (failed) wind. Instead some of the electrons emit via optically thick Comptonization of the cooler disc seed photons. This optically thick Compton emission adds to the spectrum at low energies, producing an excess of soft X-rays, hence we call the physical region producing this emission the 'soft excess'. An optically thin corona extends above the soft excess at the very smallest radii. This corona contains hot electrons at lower density and higher energy than the soft excess and provides a source of optically thin Comptonization, using seed photons from the cooler soft excess region (Jin et al. 2013).

Fig. 1(a) shows the physical locations of each model component and Fig. 1(b) shows their contributions to the total X-ray spectrum. For simplicity we approximate the geometry of the accretion flow as a flattened disc. We model the wind as a series of individual clouds which transit the flow (from left to right in Fig. 1a, corotating with the flow) and obscure the intrinsic emission. We assume identical spherical clouds. The model has five free parameters: cloud transit time, cloud radius, cloud number density, transit latitude and cloud ionization. In the following sections (Sections 2 and 3) we investigate the effect of occultations with no intrinsic variations in luminosity of the accretion flow components, i.e. we assume constant flux from the underlying accretion flow. In all cases we assume an inclination angle of the accretion flow with respect to the line of sight of 70°, BH mass of $10^7\,{\rm M}_\odot$ and define a soft band from 0.3

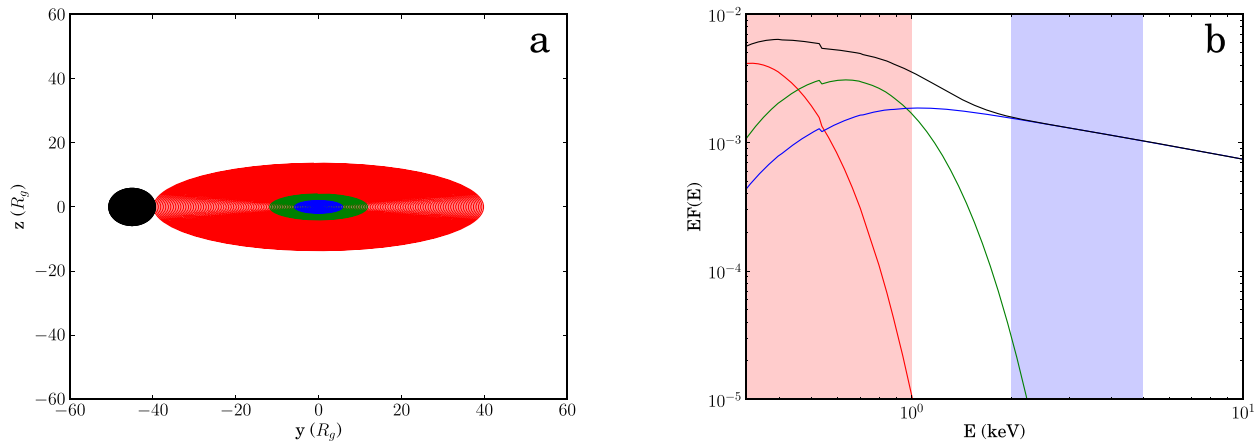

Figure 1. (a) Physical location of accretion flow model components, as viewed at high inclination ($i = 70°$): disc (red), soft excess (green), corona (blue), obscuring cloud (black). For simplicity we have approximated the geometry of the accretion flow as a flattened disc. (b) Spectrum emitted by each component, with total spectrum shown in black, and hard and soft bands shaded in blue and red, respectively.

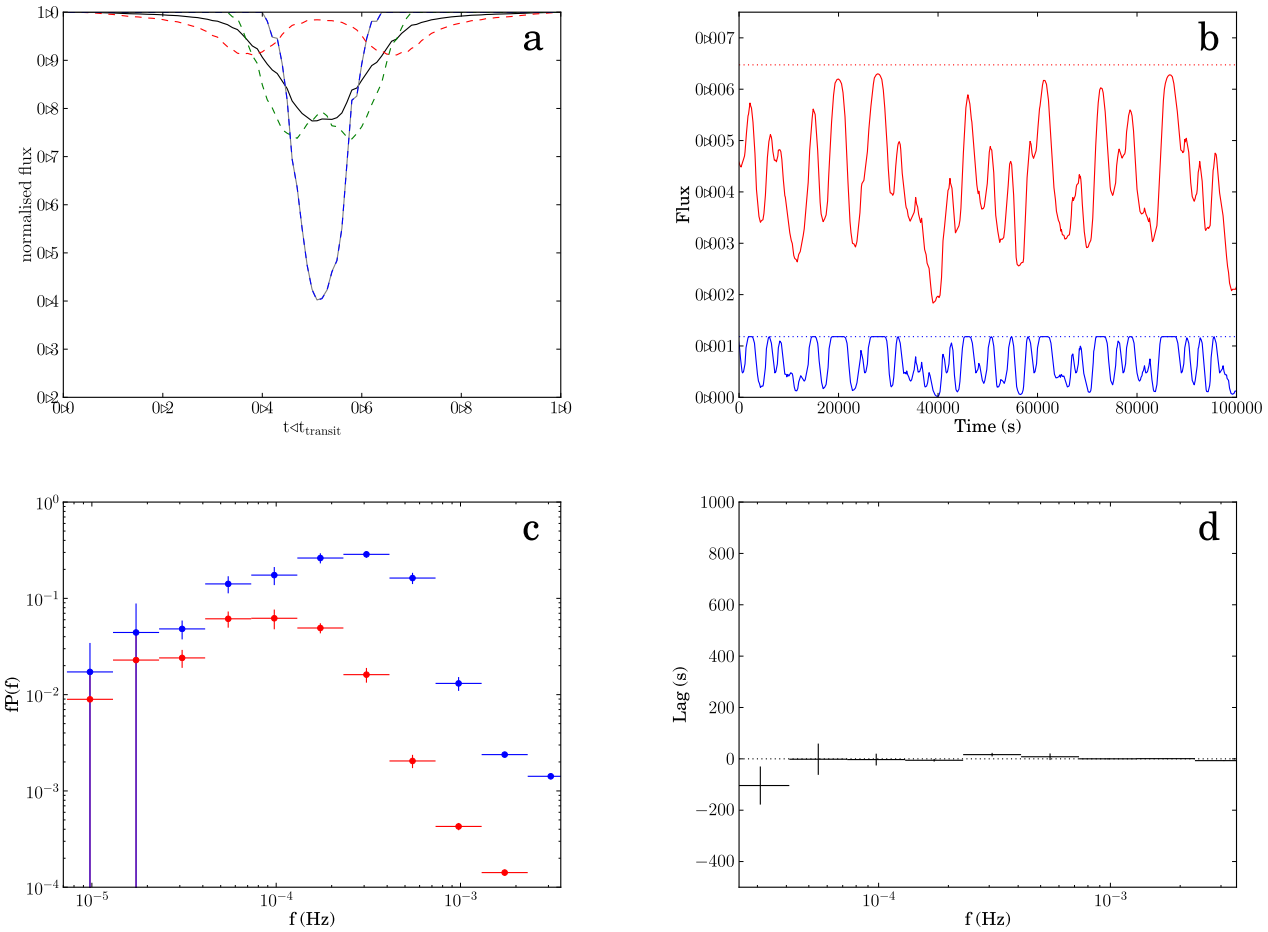

Figure 2. Model occulting a static accretion flow. (a) Fractional flux drop for a single occultation as a function of total transit time: disc (dashed red), soft excess (dashed green), corona (dashed blue), hard band (2–5 keV, solid grey; same shape as coronal flux drop), soft band (0.3–1 keV, solid black). (b) Sample hard (blue) and soft (red) model light curves, showing effect of occultations. Dotted lines show unobscured flux level. (c) Hard and soft band power spectra (blue and red, respectively). (d) Lag-frequency spectrum between hard and soft bands.

to 1 keV and hard band from 2 to 5 keV (shaded in red and blue, respectively, in Fig. 1b).

2.1 Effect of Doppler boosting

Fig. 2(a) shows the fractional flux drop as a single cloud passes across a static accretion flow. We assume the cloud reduces the observed flux by $e^{-\tau}$, where the optical depth $\tau = 1$ and does not vary with the energy of the incident radiation, i.e. the material is completely ionized.

The dashed red line shows the drop in disc flux. Since the apparent size of the disc is much larger than the cloud the drop in flux is small (<10 per cent). We assume a radial emissivity profile for the disc of $\varepsilon(r) \propto r^{-3}$, so when the cloud occults the outer parts of the disc the flux drop is small. The flux drop increases as the transit progresses and the cloud begins to occult the inner brighter disc radii. The disc flux recovers during the middle of the transit, as the cloud passes over the innermost regions occupied by the corona and soft excess, and then drops again as the cloud crosses the far side of the disc. The dashed green line shows the drop in flux from the soft excess. This shows similar behaviour, but more centrally concentrated, since the soft excess region is smaller. The corona shows the biggest drop in flux (dashed blue line), being a similar size to the occulting cloud. The solid grey and black lines show the flux drop in the hard and soft bands, respectively. The hard band is dominated by emission from the corona and hence shows a greater flux drop than the soft band, which is dominated by emission from the disc and soft excess.

Fig. 2(b) shows sample hard and soft band light curves (in blue and red, respectively), showing the effect of multiple occultations. Dotted lines show the unobscured flux levels. The light curves are generated by allocating each cloud a random start time for its transit of the disc. Each cloud has a radius of $5R_g$ and takes $T_{tr} = 10^4$ s to cross the accretion flow (from left to right as seen in Fig. 1a). On careful inspection of the light curves it can be seen that the width of the occultations is narrower in the hard band than the soft band, due to the smaller physical size of the corona, which is the main contributor of hard band flux.

Fig. 2(c) shows the corresponding power spectra. The occultations add power to the light curve at a frequency that is related to the transit time. In this simulation all clouds were given a transit time of $T_{tr} = 10^4$ s, corresponding to a frequency of 10^{-4} Hz. The power in the hard band peaks at a slightly higher frequency and greater amplitude. This is a direct result of the shape of the flux drops shown in Fig. 2(a). The more compact coronal emission experiences a narrower, deeper flux drop than the more extended soft band components, hence occultations add more power to the

hard band and at higher frequencies. The width of the hard band flux drop is $\sim 0.2T_{\rm tr} \sim 2 \times 10^3$ s, which corresponds to a frequency of 5×10^{-4} Hz. Hence the power drops off sharply above 5×10^{-4} Hz. Nevertheless there is a low power tail extending to higher frequencies in both bands. A single occultation cannot add power at these frequencies. This power comes from the superposition of occultations. The hard and soft band light curves in Fig. 2(b) show that multiple occultations close together can add variability on time-scales much shorter than that of an individual transit.

Fig. 2(d) shows the lag as a function of frequency between the hard and soft bands (calculated following Nowak et al. 1999; see also appendix of GD14). There is no lag at any frequency. This is because, even though the soft band flux drop is wider than the hard band, they are both symmetric around a common centre. Even though the soft band flux drops before the hard, the hard flux then recovers before the soft with the same time delay, cancelling out any net lag. This is the case for a stationary disc.

However, the accretion flow is not stationary. Material should be rotating at the Keplerian frequency. As a consequence material on one side of the flow is travelling towards the observer and Doppler boosted, while on the other side the emission is deboosted. Fig. 3 shows the resulting flux drops, light curves, power spectra and lags now including the effect of this Doppler boosting.

Fig. 3(a) shows that the flux drop in each component is now no longer symmetric. Doppler boosting means that the approaching side of the accretion flow appears brighter than the receding side. We assume the occulting clouds are corotating with the flow. The approaching side of the flow, which now contributes a greater fraction of the total flux, is occulted first. Hence the first half of the transit shows a much stronger flux drop. The receding side of the flow contributes much less flux to the total spectrum, hence there is a much smaller flux drop during the second half of the transit. This effect is more noticeable in the more extended components – the disc and soft excess – and most noticeable in the soft excess, where the smaller radii give faster radial velocities and stronger Doppler boosting/deboosting. The flux drops in the hard and soft bands (grey and black solid lines) are consequently skewed towards the first half of the transit, with the soft band being more strongly skewed. On closer inspection of Fig. 3(a), it can be seen that the soft band flux now drops before the hard flux *and recovers* before the hard flux. The occultations themselves have introduced a lag between the hard and soft energy bands.

Fig. 3(e) shows the lag as a function of frequency between the hard and soft energy bands. The only source of variability in the light curves is the occultations, we keep the intrinsic flux from the accretion flow constant. By including the effects of Doppler boosting, the occultations have introduced a soft lead of $\sim$300 s (a positive lag value indicates the soft band leading the hard). This lead remains roughly constant for the frequency range over which the occultations introduce power into the light curves ($\sim 5 \times 10^{-5}$–5×10^{-4} Hz).

Fig. 3(f) shows the lag as a function of energy. This is constructed by choosing a reference band (in this case the hard band, 2–5 keV) and then dividing the spectrum into a series of energy bins. The flux in each energy bin is summed up as a function of time to create a light curve for that energy bin. The light curve of the energy bin is then compared with the reference band light curve and the value of the lag between the two is computed as a function of frequency. In Fig. 3(f) we plot the value of the lag from each energy bin for two frequency ranges: low frequency (red points, 2.3×10^{-5}–7.3×10^{-5} Hz) and high frequency (blue points, 2.3×10^{-4}–7.3×10^{-4} Hz). This gives the energy spectrum of the lag at that frequency. For each energy bin, a negative lag value implies that energy bin leads the hard reference band.

At low frequencies, energy bins below 1 keV lead the hard reference band, with a lead that increases as the energy of the bin decreases (red points, Fig. 3f). These are the energies at which the disc and soft excess dominate. The soft excess emission peaks at $\sim$0.5 keV, giving way to the disc at lower energies. Since the clouds occult the outermost components first, crossing first the disc and then the soft excess before passing in front of the corona, the low energy disc emission shows the strongest lead, giving way to a slightly shorter lead from the soft excess at smaller radii and higher energies. Above 1 keV the emission is dominated by the corona. These are the energies also covered by the reference band (2–5 keV). Hence the lag of the energy bins with respect to the reference band tends to zero at high energies (>1 keV).

This pattern of soft leads (at low frequencies) is a signature normally associated with propagation; low frequency fluctuations are generated in the cooler outer components and propagate down to the hotter smaller radii which produce the high energy emission. Yet in this scenario we have produced soft leads simply by the movement of absorbing clouds, i.e. occultations affect the lag-frequency and lag-energy spectra the same way as propagation, by introducing soft leads.

Soft leads due to propagation of fluctuations are generally confined to low frequencies, since large radii only generate slow fluctuations. The blue points in Fig. 3(f) show that occultations can continue producing strong soft leads up to much higher frequencies. This is because the strength and frequency of the soft leads are no longer determined by the properties of the accretion flow but by the properties of the transiting clouds. However, comparison of the red and blue points in Fig. 3(f) shows that, while all energy bins below 1 keV show a soft lead at low frequencies, at high frequencies the two lowest energy bins (<0.3 keV) switch from a soft lead to a soft lag. These two energy bins are dominated by disc emission. High frequency variability results from short time-scale features in the flux drops shown in Fig. 3(a), implying this soft lag confined to very low energy comes from the cloud covering the deboosted side of the disc after covering the corona.

For completeness we also show the coherence between hard and soft energy bands (Fig. 3d), where 1 is perfect coherence between the two bands and 0 is incoherence. The coherence remains high up to high frequencies, since occultation is the only source of variability in the two light curves and is common to both. The coherence drops off above $\sim 5 \times 10^{-4}$ Hz, where the variability power introduced by the occultations also drops off. 5×10^{-4} Hz corresponds roughly to the width of the hard band flux drops ($\sim 0.2T_{\rm tr} \sim 2 \times 10^3$ s).

2.2 Effect of transit time

Fig. 4 shows the effect of changing the cloud transit time. We increase the transit time from $T_{\rm tr} = 5 \times 10^3$ (black) to 1.5×10^4 s (magenta). The hard band power spectra (dashed lines, Fig. 4a) clearly show that as the transit time increases, the peak frequency at which power is added to the light curves decreases. The decrease in peak frequency of $\sim$half an order of magnitude roughly matches the threefold increase in transit time. The total amount of power added to the light curves also increases by a similar amount in both bands.

Fig. 4(b) shows how this affects the lag measured between the hard and soft band light curves. For short transit times (5×10^3 s, black), a short lag ($\sim$150 s) is measured up to high frequencies (10^{-3} Hz). As the transit time increases, the maximum frequency at

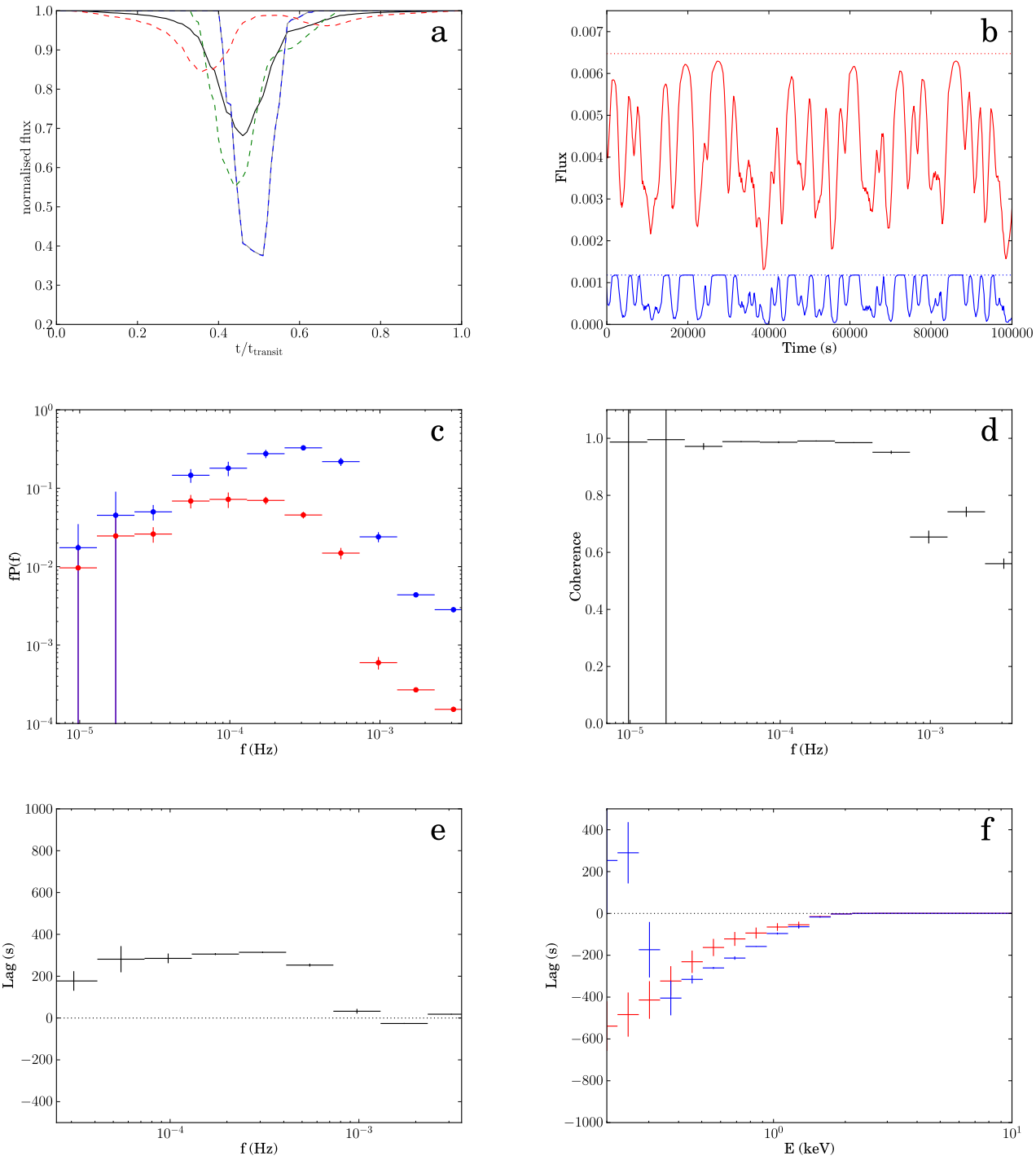

Figure 3. Occultation model including effects of Doppler boosting. (a) Fractional flux drop for a single occultation as a function of total transit time: disc (dashed red), soft excess (dashed green), corona (dashed blue), hard band (2–5 keV, solid grey; same shape as coronal flux drop), soft band (0.3–1 keV, solid black). (b) Sample hard (blue) and soft (red) model light curves, showing effect of occultations. Dotted lines show unobscured flux level. (c) Hard and soft band power spectra (blue and red, respectively). (d) Coherence between hard and soft energy bands. (e) Lag-frequency spectrum between hard and soft bands. (f) Lag-energy spectrum calculated using 2–5 keV reference band. Red points show energy spectrum of lag at low frequencies (2.3×10^{-5}–7.3×10^{-5} Hz), blue points show the lag-energy spectrum at high frequencies (2.3×10^{-4}–7.3×10^{-4} Hz).

which a lag is measured decreases. This is because occultations with a longer transit time cannot add high frequency power to the light curves (as shown by the power spectra in Fig. 4a). The absolute value of the lag also increases, since for longer transit times the clouds spend longer occulting the outer soft components before they cross and occult the central corona. The measured lag drops from ∼550 to 150 s roughly matching the decrease in transit time of a third from 1.5×10^4 to 5×10^3 s.

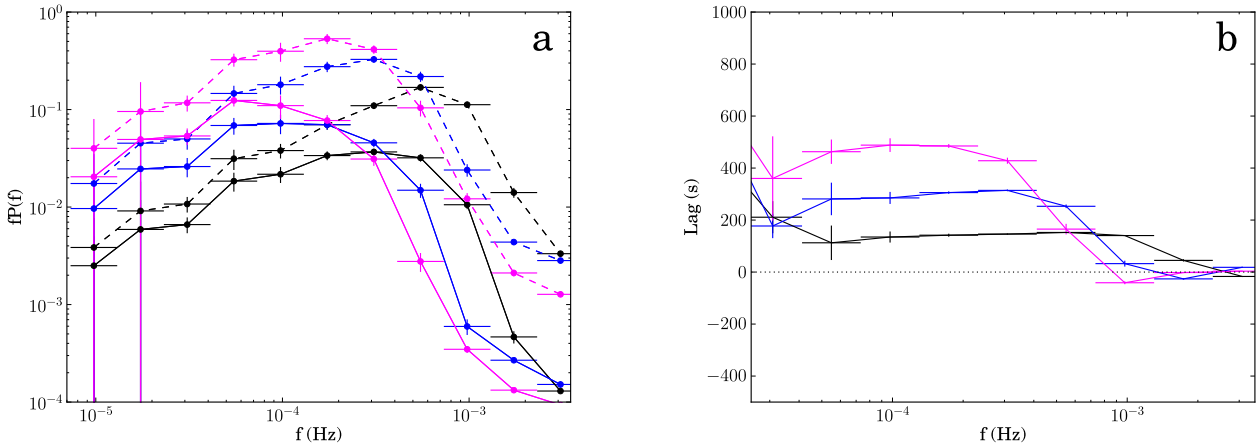

Figure 4. Effect of increasing cloud transit time on (a) power spectrum and (b) lag-frequency spectrum, for $T_{\rm tr} = 5 \times 10^3$ (black), 10^4 (blue) and 1.5×10^4 s (magenta). Solid lines show soft band (0.3–1 keV) power spectra, dashed lines show hard band (2–5 keV) power spectra.

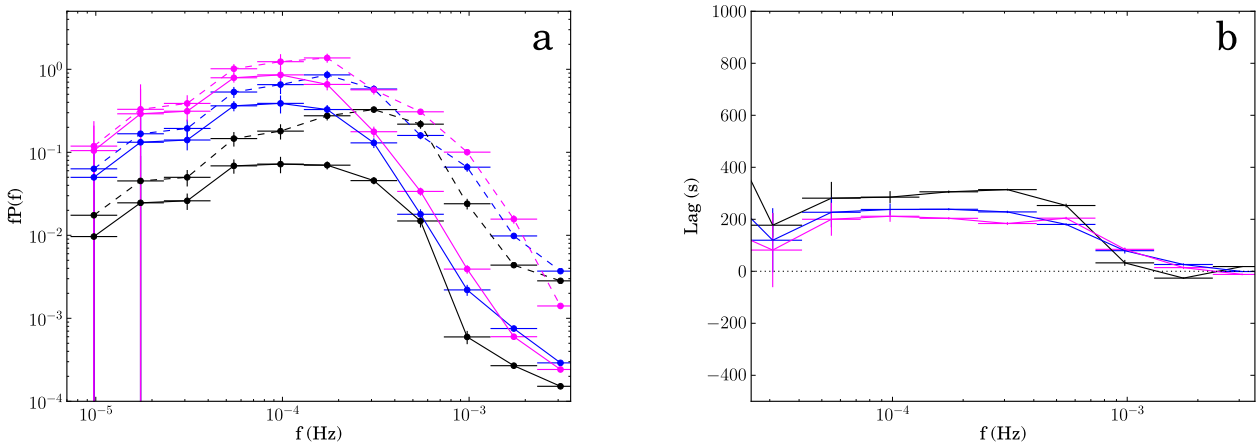

Figure 5. Effect of increasing cloud radius on (a) power spectrum and (b) lag-frequency spectrum, for $R_{\rm cl} = 5$ (black), 10 (blue) and $15R_{\rm g}$ (magenta). Solid lines show soft band (0.3–1 keV) power spectra, dashed lines show hard band (2–5 keV) power spectra.

We note that increasing BH mass or increasing the size scales of the individual components has a similar effect on the power spectrum and variability as increasing the transit time.

2.3 Effect of cloud radius

We now fix the transit time at 10^4 s and investigate the effect of changing the cloud radius. Fig. 5 shows the resulting power spectra and lag-frequency spectra for $R_{\rm cl} = 5$, 10 and $15R_{\rm g}$ (black, blue and magenta lines, respectively).

Increasing the cloud radius increases the amount of power in the light curves. The soft band shows the biggest increase (Fig. 5a, solid lines), with the amount of power at 10^{-4} Hz increasing by nearly one and a half orders of magnitude. The effect is much less in the corona-dominated hard band (just under an order of magnitude), because the corona is much smaller, so that it is already completely obscured by a small cloud of $5R_{\rm g}$. Increasing the cloud radius only prolongs the length of time it is obscured. By contrast the much larger disc is never completely obscured by a $5R_{\rm g}$ cloud. Increasing the cloud radius therefore increases the area of the disc that experiences obscuration and hence adds more power to the soft band light curve.

The more noticeable change to the hard band light curve is that the frequency at which the hard band power peaks decreases as the cloud radius increases (Fig. 5a, dashed lines). This is because, for a larger cloud radius (and fixed transit time), the time taken between covering and uncovering the corona increases. Consequently the transit cannot add as much high frequency power to the light curve. The peak in power drops from $\sim 3 \times 10^{-4}$ to 2×10^{-4}, as more power is added at low frequencies and lost at high frequencies.

Fig. 5(b) shows the lag as a function of frequency between the hard and soft band light curves. The lag measured actually slightly decreases as cloud radius increases. This is because the larger the cloud, the more time it spends obscuring hard and soft components simultaneously. This results in very broad, very similar flux drops in both the hard and soft bands. In contrast, the strongest soft leads are seen when the cloud is small enough to obscure the blue wing of the disc and soft excess and then the corona in turn. This results in much narrower flux drops in the hard and soft bands, where the skew due to Doppler boosting (which causes the soft lead) is much more prominent.

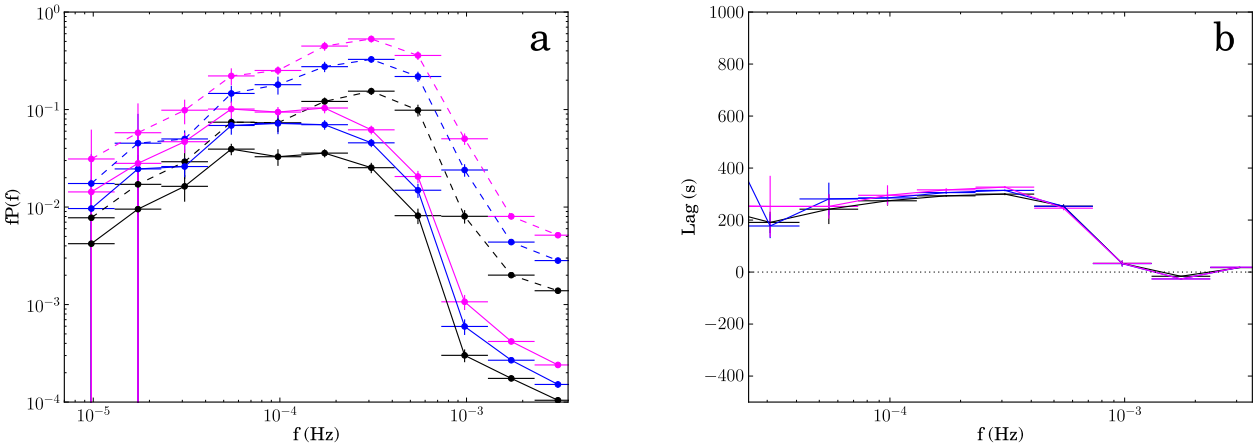

Figure 6. Effect of increasing number of clouds on (a) power spectrum and (b) lag-frequency spectrum, for $n_{\rm cl} \sim 5 \times 10^{-4}$ (black), 10^{-3} (blue) and 1.5×10^{-3} s^{-1} (magenta). Solid lines show soft band (0.3–1 keV) power spectra, dashed lines show hard band (2–5 keV) power spectra.

2.4 Effect of cloud number density

Fig. 6 shows the effect of increasing the number of occulting clouds. We fix the cloud radius and transit time at $5R_{\rm g}$ and 10^4 s and increase the number density of clouds from $n_{\rm cl} \sim 5 \times 10^{-4}$ (black) to 1.5×10^{-3} s^{-1} (magenta). Our total simulation time is 1.024 Ms, in practice this corresponds to increasing the total number of occulting clouds from 500 to 1500 clouds, each of which is assigned a random start time for its transit.

Fig. 6(a) shows that increasing the number of clouds increases the power spectrum normalization without affecting its shape. This is because more occultations simply add more power to the light curve. Both the hard and soft bands are affected equally. Fig. 6(b) shows that increasing the number of occultations has no effect on the lag measured between the hard and soft band light curves. The value of the lag is determined primarily by the transit time, with a weak dependence on cloud radius.

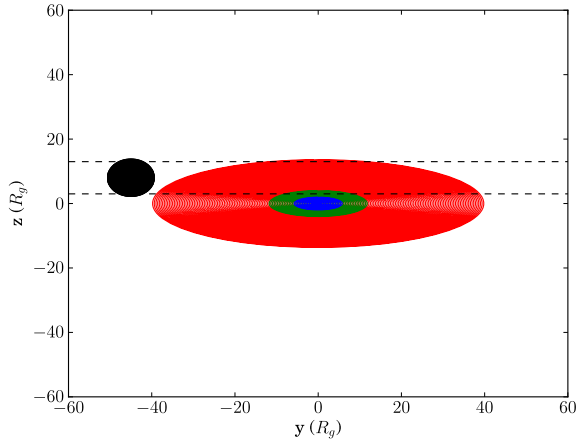

Figure 7. Dashed lines show path of cloud across accretion flow for a high transit latitude ($z_{\rm cl} = 8$), with disc (red), soft excess (green), corona (blue), obscuring cloud (black) and accretion flow viewed at $i = 70°$.

2.5 Effect of transit latitude

In Fig. 8 we show the effect of increasing the latitude of the cloud path so that it no longer aligns exactly with the BH. In all three cases we fix the cloud radius and transit time to $5R_{\rm g}$ and 10^4 s and the number density of clouds to 10^{-4} s^{-1}. We increase the apparent latitude of the cloud centre from $z_{\rm cl} = 0$ to 8. Fig. 7 shows as an illustration the path taken by a cloud transiting at $z_{\rm cl} = 8$, where the dashed lines bound the region experiencing obscuration.

Fig. 8(a) shows the effect on the hard and soft band power spectra. As the latitude increases the cloud only obscures the 'back half' of the accretion flow ($z > 0$ in Fig. 7). Consequently the power in the light curves decreases. By the time the latitude has increased to $8R_{\rm g}$ the cloud no longer obscures the central corona, hence there is almost no power in the hard band (hence no dashed magenta line), since we have fixed the underlying accretion flow to have constant flux. Consequently high latitude transits that do not occult the corona add power to the soft band that is uncorrelated with the hard band.

The soft band power drops from $\sim 7 \times 10^{-2}$ for a central transit (solid black line) to $\sim 10^{-3}$ at the highest latitude (solid magenta line). Comparison of the black and magenta solid lines shows that not only has total power been lost, but also power has preferentially been lost at high frequencies. Below 5×10^{-5} Hz the two soft band power spectra show the same shape, whilst above 5×10^{-5} Hz the high latitude power spectrum shows a cut-off, with the power dropping off sharply above 10^{-4} Hz. This is because the transiting cloud just clips the very edge of the disc and soft excess. These regions of the flow are travelling nearly perpendicular to the line of sight so experience very little Doppler boosting/deboosting. They therefore carry only a moderate fraction of the total soft band flux. The shortest, sharpest dips in the soft band light curve arise through the cloud occulting the innermost parts of the disc/soft excess, which are centrally concentrated and strongly Doppler boosted. These add the highest frequency components to the soft band light curve. Occultations of the outer parts of the flow result in slower more gradual flux drops and hence add low frequency power. The coronal power law also contributes some flux to the soft band, so with no coronal occultations that removes its additional source of high frequency power.

Fig. 8(b) shows the effect of increasing the transit latitude on the lag measured between the hard and soft bands. As high frequency power is lost from both the hard and soft bands, the measured lag begins to tend to zero at lower frequencies ($\sim 2 \times 10^{-4}$ Hz for

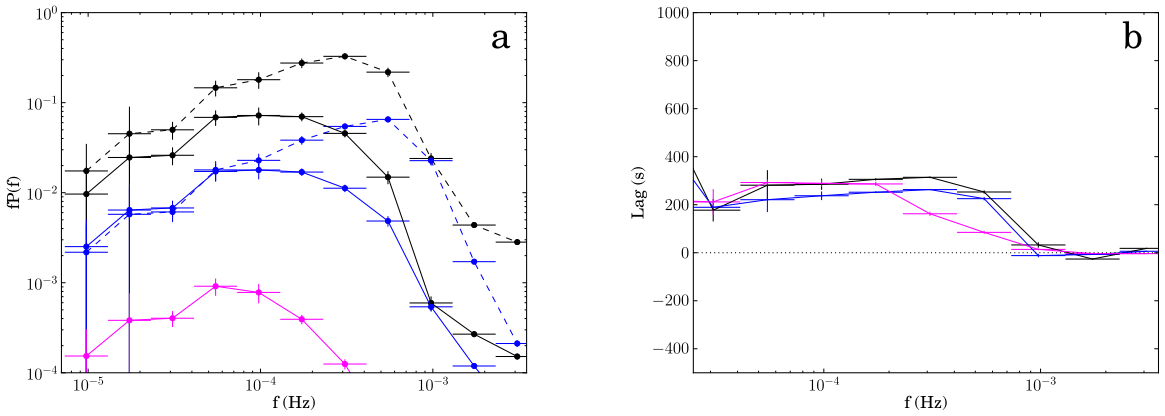

Figure 8. Effect of increasing transit latitude on (a) power spectrum and (b) lag-frequency spectrum, for $z_{\rm cl} = 0$ (black), 5 (blue) and $8R_{\rm g}$ (magenta), where $z_{\rm cl}$ defines the apparent latitude of the centre of the clouds as shown in Fig. 1(a). Solid lines show soft band (0.3–1 keV) power spectra, dashed lines show hard band (2–5 keV) power spectra.

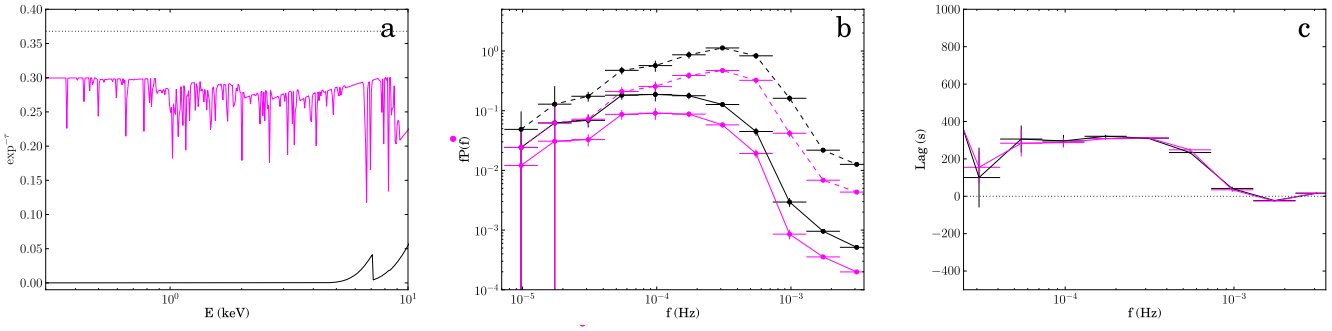

Figure 9. Effect of changing cloud ionization on (a) transmission spectrum, (b) power spectrum and (c) lag-frequency spectrum, for two cloud ionization states: $\xi = 0$ (black) and $\log \xi = 4$ (magenta). Solid lines show soft band (0.3–1 keV) power spectra, dashed lines show hard band (2–5 keV) power spectra. Dotted line shows transmitted flux level for constant $e^{-\tau}$, $\tau = 1$.

the high latitude magenta spectrum, compared to 7×10^{-4} Hz for the central transit back spectrum). The lag tends more gradually to zero in the case of the high latitude transit. This is again because the highest frequency components come from the shortest, sharpest flux drops which arise from occulting the brightest central regions. For a high latitude transit this is when the cloud just clips the small part of the soft excess that appears at high latitude (i.e. large z and $y = 0$ in Fig. 7) at the midpoint of the transit. Because the coronal flux is not occulted, occultation of the soft excess is the only source of variability in the hard band. It is also the only source of high frequency variability in the soft band. When the source of variability is the same in both bands, there can be no lag between them. Hence as frequency increases above $\sim 2 \times 10^{-4}$ Hz the lag tends gradually to zero as the only source of variability becomes occultation of the soft excess in both bands.

2.6 Effect of cloud ionization

So far we have approximated the absorption of the cloud as $e^{-\tau}$, where the electron scattering optical depth, $\tau = 1$ (equivalent to a pure hydrogen column of 1.5×10^{24} cm^{-2}, which is 1.25×10^{24} cm^{-2} for solar abundance material), is a constant with energy. However this is only appropriate for completely ionized material. In general, the optical depth of the cloud is a function of energy, depending on the ionization state of the cloud.

In Fig. 9(a) we show our original model (dotted black line) compared to transmission spectra for $N_{\rm H} = 1.5 \times 10^{24}$ cm^{-2} at $\log \xi = 4$ (magenta line) and at $\xi = 0$ (solid black line). The $\log \xi = 4$ transmission spectrum is calculated using the XSPEC model ZXIPCF. This assumes a turbulent velocity of 200 km s^{-1}, so the line strength can be enhanced for the same column density of material for higher velocities. The neutral spectrum is calculated using PHABS. As before, we fix $R_{\rm cl} = 5R_{\rm g}$, $T_{\rm tr} = 10^4$ s, $n_{\rm cl} = 10^{-4}$ s^{-1} and $z_{\rm cl} = 0$. Having fixed both the optical depth and cloud radius, this constrains the cloud density, since $n = \tau/(2R_{\rm cl}\sigma_{\rm T}) \sim 10^{11}$ cm^{-3}. The ionization state of the clouds is related to their density and the X-ray luminosity as $\xi = L_{\rm X}/(nD^2)$, where D is the distance of the cloud from the central X-ray source. For $L_{\rm X} = 10^{42}$ erg s^{-1} and $D = 20R_{\rm g}$, $\xi \sim 10^4$.

Fig. 9(b) shows that increasing the ionization state of the cloud reduces the amount of power added to the hard and soft band light curves. The difference is roughly half an order of magnitude in both bands, since the change in opacity is roughly the same for both bands. For a neutral cloud, the transmitted flux below 5 keV is zero. In contrast, when the cloud is highly ionized there is very little absorption left, so the fraction of transmitted flux rises to $e^{-\tau} \sim 0.3$. This results in shallower flux drops and hence less power in the hard and soft band light curves.

Fig. 9(c) shows that changing the ionization state of the clouds has no effect on the lag measured between the hard and soft energy bands. The lag depends on the motion of the cloud with time, not on the relative amounts of power carried by the hard and soft bands.

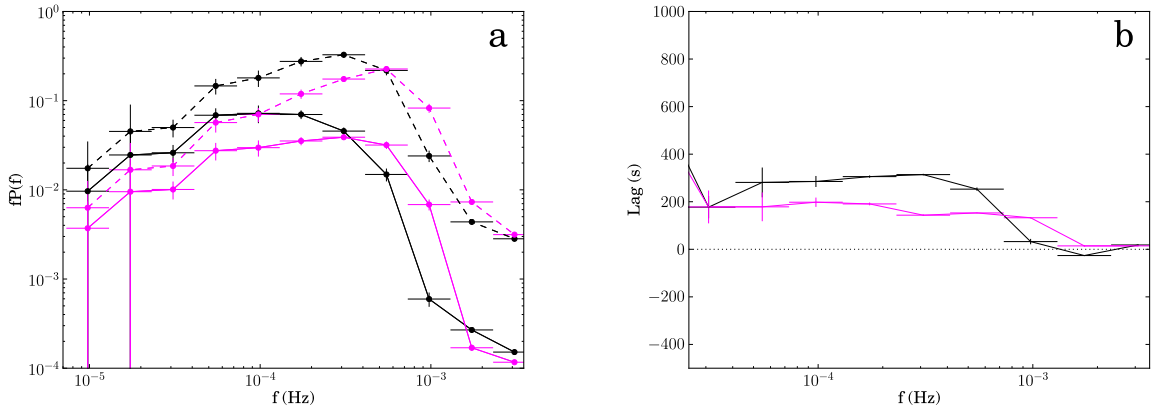

Figure 10. Change in (a) power spectrum and (b) lag-frequency spectrum when circular motion of clouds is taken into account (magenta), compared with linear occultations (black). Solid lines show soft band (0.3–1 keV) power spectra, dashed lines show hard band (2–5 keV) power spectra.

3 CIRCULAR OCCULTATION

So far we have modelled linear occultations, where the apparent velocity of the clouds remains constant during the transit. However the clouds should be rotating with the accretion flow, in which case their apparent velocity during the transit will vary as a cosine function. During the middle of the transit the component of the cloud's velocity perpendicular to the line of sight is greatest and the cloud appears to move faster. At the beginning and end of the transit the cloud is moving towards/away from the observer, the component of its velocity perpendicular to the line of sight is small and its apparent velocity is much slower. If the orbital radius of the clouds is much larger than the radius of the region being occulted, then linear occultation is a reasonable approximation. As the orbital radius of the clouds becomes similar to the occulting region size the effect becomes more important. A transit time of 10^4 s corresponds to a Keplerian orbital velocity at $\sim 20R_g$ for a 10^7 $M_\odot$ BH, implying this effect should be taken into account.

Fig. 10 shows the effect on the power spectra and lag-frequency spectrum. We fix $R_{cl} = 5R_g$, $T_{tr} = 10^4$ s, $n_{cl} = 10^{-4}$ s^{-1} and $z_{cl} = 0$ and show the result of linear occultations in black and accounting for circular motion in magenta. In the circular case the cloud moves faster while it is occulting the brightest central region of the accretion flow. As a result the flux drops are narrower. This adds more power at higher frequencies, hence both the hard and soft band power spectra are shifted to slightly higher frequencies for the case of circular occultations (Fig. 10a).

Similarly the lag-frequency spectrum extends to slightly higher frequencies in the circular motion case, showing a non-zero lag up to 10^{-3} Hz compared to 7×10^{-4} Hz for linear occultations (Fig. 10b). The measured lag is also shorter ($\sim$200 s compared to 300 s for linear occultations). Again this is a consequence of the cloud moving faster during the central part of the occultation. The lag predominantly arises from the delay between occulting soft excess and then coronal emission on the Doppler boosted side of the flow and when the cloud is moving faster the delay is shorter.

4 TRANSITION FROM SIMPLE TO COMPLEX NLS1 BY INCLUDING OCCULTING CLOUDS

We now investigate whether the addition of occultations can change the timing properties of a simple NLS1 so that they appear more typical of complex NLS1s. That is, can the effect of occultations reduce the maximum measured reverberation lag from $\sim$200 s to nearer 50 s and shift it to higher frequencies?

In the previous sections we assumed constant flux from the underlying accretion flow. We now replace this static model with the time-dependent model of GD14 shown in Fig. 11(a). The disc, which is at the largest radii, generates the slowest fluctuations. These propagate down to the soft excess, which is at smaller radii and generates its own slightly faster fluctuations. The fluctuations in soft excess emission therefore consist of the slow fluctuations from the disc, delayed by some lag related to the propagation time, modulated by the faster fluctuations generated in the soft excess. These fluctuations then propagate down to the corona, which generates even faster fluctuations. The hard coronal emission therefore shows fluctuations on a whole range of time-scales, as it responds to mass accretion rate fluctuations propagating down from all radii. A fraction of these central hard X-rays will illuminate the cooler soft excess and disc components. Some of this illuminating flux will be reflected, the rest will thermalize and be reprocessed. Fig. 12 shows our spectral decomposition now including these reflected and reprocessed components. These come from a fit to the time averaged spectrum of the simple NLS1 PG 1244+026 (obd id: 0675320101, see GD14), shown in black data points. For simplicity we assume all reflection/reprocessing occurs on the soft excess (6–$12R_g$). Thus the fluctuations in the reflected/reprocessed emission follow the coronal fluctuations (Fig. 11a), except for the very fastest fluctuations which are smoothed out by the range of light travel time delays. Hence the reflected and reprocessed fluctuations are a lagged and smoothed version of the hard coronal fluctuations. The soft excess therefore consists of intrinsic emission from the accretion flow (dashed green line, Fig. 12), which varies slowly due to intrinsic mass accretion rate fluctuations in the soft excess and those that have propagated inwards from the disc, and reprocessed emission (dotted green line, Fig. 12) which follows the faster coronal fluctuations. GD14 showed that this model can reproduce all the observed timing properties of the simple NLS1 PG 1244+026.

We use this model to describe the emission from the underlying accretion flow as a function of time, and now add the effect of occulting clouds. We fix the cloud parameters to $R_{cl} = 5R_g$, $T_{tr} = 10^4$ s and $z_{cl} = 0$. A transit time of 10^4 s implies an orbital radius of $20R_g$. Hence we reduce our transit radius from $40R_g$ in Fig. 1(a) to $20R_g$ and take into account the circular motion of the clouds. Since the clouds are launched so close to the central X-ray source we allow them to be highly ionized and use the magenta transmission

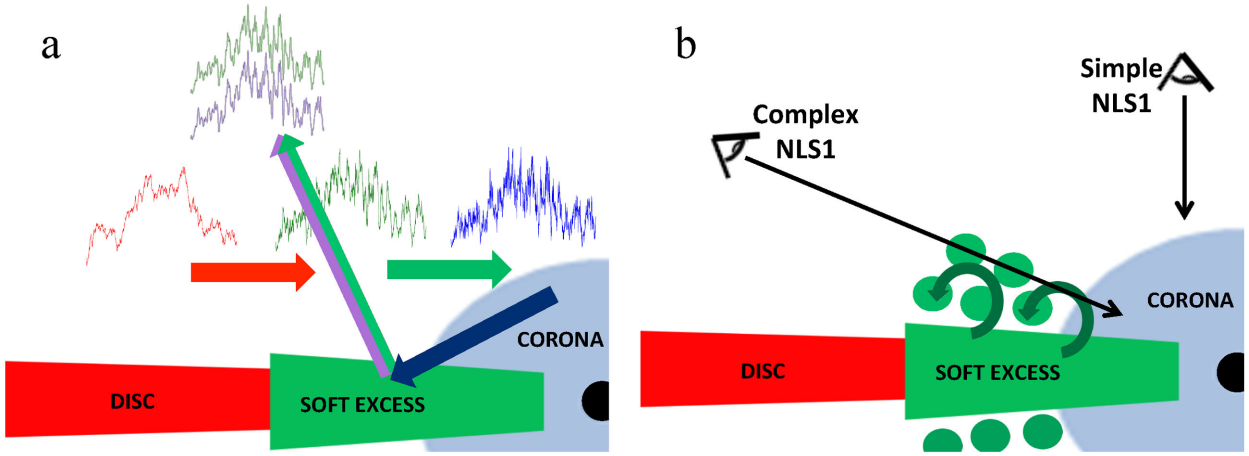

Figure 11. a). Schematic of simple NLS1 model of GD14. Slow fluctuations propagate inwards from the outer components and are modulated by the faster fluctuations generated at smaller radii. The high energy coronal emission then reflects off and is reprocessed by the soft excess component. (b) Scenario for transition from simple to complex NLS1 as a function of inclination, where the soft excess is a turbulent region of rotating clouds which partially obscures the line of site to the central regions in complex NLS1s. The clouds are then responsible for the bulk of the reflected/reprocessed emission, while partially obscuring the intrinsic emission.

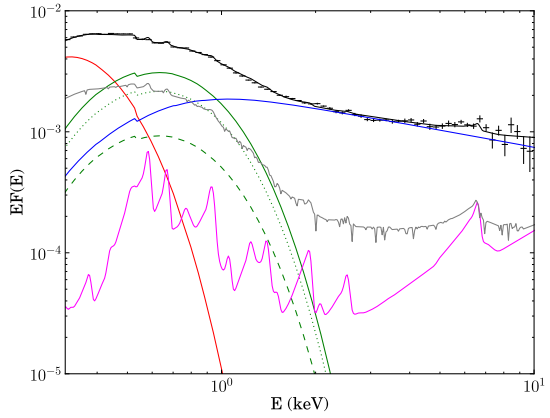

Figure 12. Spectral decomposition for PG 1244+026: disc (red), soft excess (green, with dashed line for intrinsic emission, dotted line for reprocessed emission, solid line for total), corona (blue), reflection (magenta), total (black). Data points show time averaged spectrum (obs id: 0675320101). Grey line shows an example of the spectrum after introducing absorption by intervening clouds.

spectrum shown in Fig. 9(a) ($\log \xi = 4$, $N_{\rm H} = 1.5 \times 10^{24}\,{\rm cm}^{-2}$). $20R_{\rm g}$ is consistent with the clouds being launched as part of a failed Eddington (radiation pressure driven) wind from the soft excess region as sketched in Fig. 11(b). Radiation pressure lifts material from the accretion flow, which forms clumps as it rises (Takeuchi, Ohsuga & Mineshige 2014). As soon as the optical depth of the clumps becomes $\tau > 1$, some of the material is self-shielded from X-ray photons. The mass of the clump is still the same but the radiation pressure on it is now less. If the source is not strongly super-Eddington, the radiation pressure is not strong enough to expel the material so it falls back to the disc, resulting in a failed rather than outflowing wind. The whole turbulent large scale height region is the source of the soft excess. Propagation of fluctuations occurs through the disc regions which are the source of the intrinsic emission, while the bulk of the reflected and reprocessed emission comes from the turbulent clouds. We assume the turbulent velocity is less than the orbital velocity ($v_{\rm turb} < v_{\rm Kepl}$) and that the clouds remain largely intact on the time-scale of a single transit (although $v_{\rm Kepl}$ may be sufficient to shred them on longer time-scales, stripping off material before what remains falls back to the disc). For a source at high inclination, these clouds will intercept the line of sight to the central regions. As the clouds transit the line of sight, we assume they obscure the intrinsic disc, intrinsic soft excess and coronal emission. We do not obscure the reflected or reprocessed emission, since we assume these are predominantly from the clouds.

4.1 Fourier timing properties

Fig. 13 shows the resulting soft and hard band light curves (left and right, respectively). The top panels show the original simple NLS1 model with no occultations. These light curves have power spectra that match the hard and soft band power spectra of the simple NLS1 PG 1244+026. In the subsequent panels we increase the number of occulting clouds ($n_{\rm cl} = 10^{-4}$, $10^{-3}\,{\rm s}^{-1}$). The occultations are most obvious in the hard band, where the flux drops are conspicuously narrower than in the soft band, due to the smaller physical size of the corona compared to the more extended soft band components. These occultations add power to the light curve. The most heavily occulted hard band light curve (bottom right-hand panel) shows peaks and deep troughs more typical of a complex NLS1.

Fig. 14 shows the power spectra, lag-frequency spectra and coherence between hard and soft bands for the same three simulations. Comparing the hard band power spectra (Fig. 14a, dashed lines) of the original model (black) with the most heavily obscured model (magenta) shows that occultations have increased the power at $\sim 3 \times 10^{-4}$ Hz by almost one and a half orders of magnitude. Hard band power spectra of complex NLS1s routinely show similarly high power at these frequencies. Thus occultations are more than capable of increasing the hard band high frequency power from $fP(f) \sim 10^{-2}$ typical of a simple NLS1 to $\sim$0.1 as is typical of a complex NLS1. The power increase in the soft band (solid lines) is much smaller ($\sim$half an order of magnitude). However, we have only included occultations at $z_{\rm cl} = 0$. Higher latitude occultations would add additional power to the soft band, however, this power would be uncorrelated with the hard band.

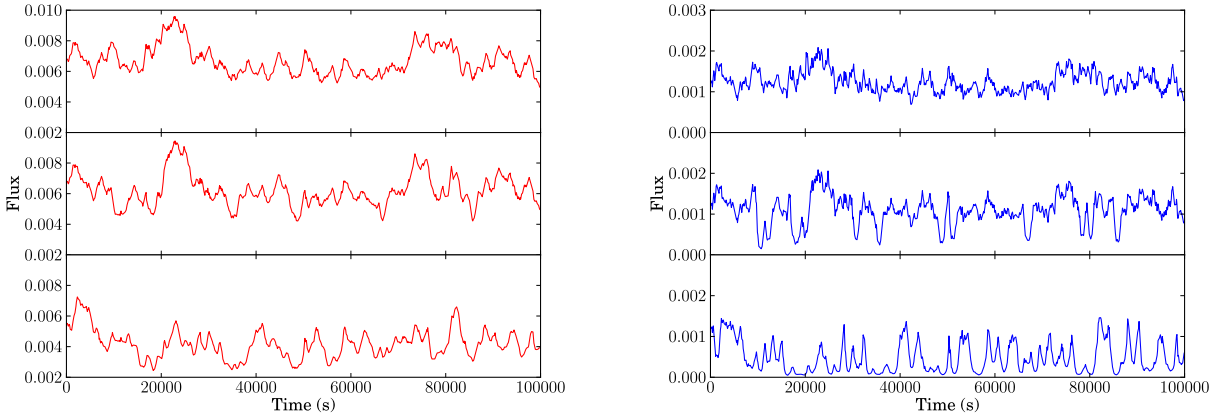

Figure 13. Soft band (0.3–1 keV, left-hand panel) and hard band (2–5 keV, right-hand panel) light curves showing effect of adding obscuring clouds to the simple NLS1 model of GD14. Top panel: simple NLS1 model with no clouds. Middle panel: $n_{\rm cl} = 10^{-4}$ s^{-1}. Bottom panel: $n_{\rm cl} = 10^{-3}$ s^{-1}. For both cases we fix the cloud parameters to $R_{\rm cl} = 5R_{\rm g}$, $T_{\rm tr} = 10^4$ s, $z_{\rm cl} = 0$, $\log \xi = 4$ and $N_{\rm H} = 1.5 \times 10^{24}$ cm^{-2} and assume the clouds are launched from $\sim 20R_{\rm g}$.

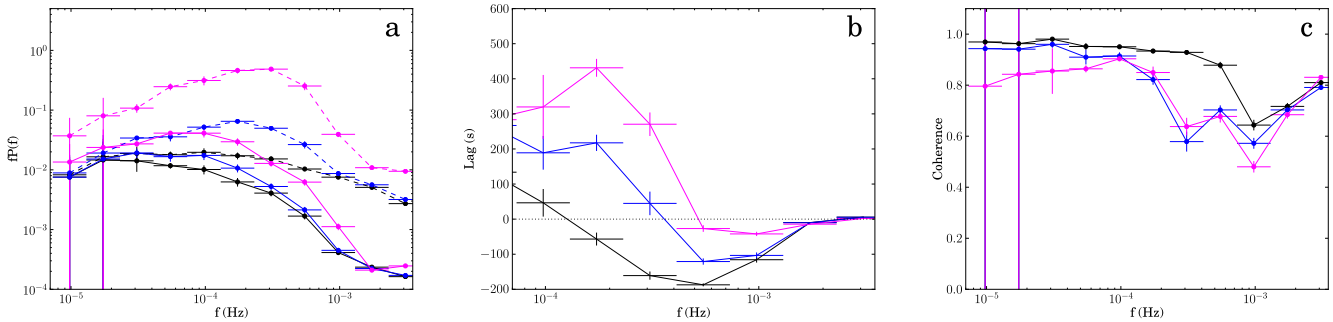

Figure 14. Effect of adding occultations to the simple NLS1 model of GD14 on (a) hard band (2–5 keV, dashed lines) and soft band (0.3–1 keV, solid lines) power spectra, (b) lag-frequency spectrum and (c) coherence between hard and soft bands. Black lines show simple NLS1 model with no clouds, blue $n_{\rm cl} = 10^{-4}$ and magenta $n_{\rm cl} = 10^{-3}$ s^{-1}, with cloud parameters as in Fig. 13.

Fig. 14(b) shows the lag as a function of frequency between the hard and soft bands. The black points show the original simple NLS1 model, with a strong reverberation lag of $\sim$200 s at $\sim 5 \times 10^{-4}$ Hz, matching that seen in PG 1244+026. As the number of occultations increases (blue to magenta), the maximum measured reverberation lag decreases from 200 to 50 s and increases in frequency from $\sim 5 \times 10^{-4}$ to 10^{-3} Hz. This much shorter reverberation lag, at higher frequency, is much more typical of those seen in complex NLS1s such as 1H 0707−495. In our model, this is a direct result of the soft leads introduced by the occultations at low frequencies, diluting the reverberation lag and shifting its minimum to higher frequencies. This is also in good agreement with the findings of Kara et al. (2013), who showed that the reverberation lag of the complex NLS1 IRAS 13224−3809 is much shorter and at higher frequency during low flux periods (when in this scenario it would be more obscured) than high flux periods.

Fig. 14(c) shows the coherence between hard and soft bands. As the number of occultations increases, the coherence drops slightly, particularly at low frequencies (from $\sim$1 to $\sim$0.8). This is due to the slightly different shaped flux drops in the hard and soft bands. The sudden drop in coherence at 10^{-4} Hz, characteristic of the simple NLS1 PG 1244+026, becomes less obvious in the more obscured simulations. The coherence functions of complex NLS1s do show a more gradual drop in coherence with increasing frequency, so this is not in disagreement with the data.

4.2 Spectral changes

In Fig. 12, in grey, we show an example of the total spectrum when the source is highly absorbed. We assume the clouds are the source of the reflected and reprocessed emission, hence these components are not absorbed. Consequently the low flux spectrum is dominated by reprocessed emission at low energies (<1 keV) and reflected emission at high energies This gives a total spectrum that is no longer power law like but instead shows strong curvature, with a large soft excess and a strong iron emission line, but the 'smoking gun' signature of highly ionized occultation is the presence of highly ionized Fe Kα absorption lines at 6.7 and 6.95 keV. The strength of these features is probably underestimated in our model as the ZXIPCF model used assumes a turbulent velocity of only 200 km s^{-1}, which is probably much smaller than expected in a failed wind structure from the inner disc.

Strong highly ionized absorption lines are detected in the deep dip states of several complex NLS1 such as Mrk 766 (Miller et al. 2007), MCG 6-30-15 (Miller et al. 2008) and Mrk 335 (Gallo et al. 2013). It is possible that even higher turbulent velocities in the failed wind could merge the 6.7 and 6.95 keV absorption lines into each other, and into the absorption edge, which could produce the more dramatic drop at Kα in 1H 0707−495 (Hagino et al., in preparation).

Our assumption that the clouds do not occult the reflected and reprocessed emission sets a limit to the amount of absorption present in our model. Complex NLS1s often show rather stronger drops at

low energy, which in this scenario would require that the clouds do also occult part of the failed wind structure or that our reprocessed emission is overestimated due to our models taking only the model flux rather than weighting this by the instrument response. Nonetheless, this model demonstrates the potential of this scenario to match the spectral variability, given a more sophisticated prescription for the reflected/reprocessed flux.

5 DISCUSSION

We have shown that occultation of the accretion flow can introduce lags between the hard and soft energy bands. In particular the occultations generate soft leads at a frequency related to the transit time. For a transit time of 10^4 s, corresponding to an orbital radius of $20R_g$, these lags predominate at low frequencies ($\sim 10^{-4}$ Hz for a 10^7 $M_\odot$ BH). When combined with a model for the intrinsic variability of the accretion flow, these low frequency soft leads act to dilute the negative reverberation lag, reducing the maximum measured lag and shifting it to higher frequencies, reproducing the trend seen in the data from simple to complex NLS1. This can plausibly be produced by increasing inclination with respect to a clumpy, turbulent structure above the inner disc. Since NLS1s are high accretion rate sources, it is likely that the inner regions of the disc will become 'puffed up' to a large scale height where the local accretion rate exceeds the Eddington limit (e.g. Jiang et al. 2014), producing a turbulent structure capable of obscuring the innermost regions. Low inclination sources are rarely occulted (simple NLS1), while high inclination ones have multiple occultations (complex NLS1). The assumed higher inclination for complex NLS1s also explains the observed association of extreme (deep dip) spectra with warm absorbers. This is not causal, in that the warm absorbers are not distorting our view of the extreme spectra (e.g. Chiang & Fabian 2011), but is instead a consequence of high inclination so that the line of sight is more likely to intercept a wind driven from the torus/flattened broad-line region (BLR). Importantly, the occultations superimpose highly ionized absorption lines at Fe Kα in the dips, as are seen in the data.

We show the evolution of the lag-frequency with increased occultations for a fixed BH mass of 10^7 $M_\odot$, but this should also depend on BH mass. The intrinsic lags/leads in the spectral components should scale simply with mass, as should the occultation time-scale. However, mass for NLS1s is hard to determine accurately, as they are accreting close to Eddington. Masses estimated from line widths assume the BLR clouds are virialized. However, the effective gravity experienced by the clouds will be reduced due to radiation pressure from the central source, leading to an underestimate for masses of NLS1s (Marconi et al. 2008). Inclination is also another uncertainty, as the BLR velocity field is not completely virialized, but contains a clear equatorial component (e.g. Collin et al. 2006; Kollatschny & Zetzl 2013; Pancoast, Brewer & Treu 2014). Any equatorial component to the velocity field will be suppressed in low inclination (simple) NLS1s, so their masses will be systematically biased towards higher values compared to high inclination (complex) NLS1s.

Leighly (1999) gives the full width at half-maximum (FWHM) for the Hβ line widths in PG 1244+026 and 1H 0707−495 as 830 and 1050 km s^{-1}, respectively. These are corrected for Fe II and have the narrow Hβ component subtracted assuming that this is 0.1 times the [O III] line intensity (see also Leighly & Moore 2004). Both sources have intrinsic optical luminosities which are very similar, so these give masses which are 2.4×10^6 and 3.7×10^6 $M_\odot$, respectively (Nikołajuk, Czerny & Gurynowicz 2009). The two object masses may be even closer if the inclination dependence discussed above is important. An Eddington correction to the mass of PG 1244+026 increases the mass estimate to 10^7 $M_\odot$ (Done et al. 2013), but this should also be similar for 1H 0707−495. Hence, while there are large uncertainties on masses for NLS1s, these two objects should be very similar. At this larger mass, PG 1244+026 is at the Eddington limit for a low spin BH (Done et al. 2013). A lower mass and/or higher spin pushes the system to higher Eddington fractions, so making it even less likely that the disc is flat.

Our model is more of a pilot study than a complete description. Obvious improvements are to include general relativistic effects of light bending on the disc image (Fig. 1a; e.g. Miniutti, Agís González & Sanfrutos Carreras 2014; Middleton & Ingram 2015). This would be most important for the central coronal regions as the far side of this small source always has a small impact parameter with the BH. This would make the corona appear larger, so a $5R_g$ cloud may not occult the entire corona. As a consequence the coronal flux drops would not be quite as narrow and deep and this would reduce the difference between the total amount of power added to the hard and soft bands. Complex NLS1s do show more power in the hard band than the soft band (Zoghbi, Uttley & Fabian 2011) at all frequencies, unlike the simple NLS1 PG 1244+026, which shows comparable power at low frequencies in the hard and soft bands. Our occultation model replicates this, since occultations add power to both bands. However, the small size of the corona necessarily adds much more power to the hard band. Including light bending (or a smaller cloud size) would slightly lessen this difference, in better agreement with the data.

The model presented here is in some way a composite between the previous extreme relativistic reflection models and partial covering models. It follows the partial covering model in identifying absorption (as opposed to light bending) events as the origin for the deep dips, but has the occulting material be closer to the source (10 gravitational radii rather than a few tens to hundreds), and be more highly ionized. Reflection does make an important contribution to the spectrum during the dips in our model, but it is not extremely smeared by relativistic effects. Instead, and in a step beyond what is modelled here, we envisage the reflector as a clumpy, turbulent, failed wind rather than a flat Keplerian disc (see also Miller et al. 2008). The clumps may be only marginally optically thick, so their reflected/scattered emission is not quite the same shape as from $\tau \gg 1$ (Miller & Turner 2013), and they may be embedded in hotter material which Comptonizes the reflected emission. Additionally, the cloud itself could have complex structure due to the ionization instability of X-ray illuminated material (Krolik, McKee & Tarter 1981). The illuminated face of the cloud will be heated to the local Compton temperature ($\sim 10^6$ K). Temperature decreases at larger depths into the cloud where scattering reduces the heating, so the density must increase to keep in pressure balance. This lower ionization state material has more line cooling, so the temperature drops abruptly, giving a sharp transition between a highly ionized skin and a nearly neutral core (Chevallier et al. 2006). Reflection from such structures, especially with a turbulent velocity field, may be a feasible way to reproduce the observed 2–10 keV spectra in the dips.

Another difference between this model and standard relativistic reflection is that we include thermalization of the illuminating flux. Hard X-rays which are not reflected can either heat the disc and be re-emitted as (mostly) thermalized radiation, or the energy can be released as lines/recombination continua. The relative importance of these two processes depends strongly on the vertical structure of the disc. Thermalization is more important for discs in hydrostatic

equilibrium (Nayakshin & Kallman 2001) but current reflection models are calculated for constant density discs (e.g. Ross & Fabian 2005; García et al. 2013). The high disc temperatures expected in NLS1s means that this component must be important at some level in contributing to the soft X-ray excess in these objects, and since it is predominantly thermal then it has no strong soft X-rays lines which require high spin to smear them into the observed smooth continuum.

However, probably the most important effect which should be included in matching to real data is that the light curves in the soft and hard bands are weighted by the detector response rather than being simply flux integrated over the energy band as used here. This is a key requirement to fit the model to real data, which will be the subject of a subsequent paper.

6 CONCLUSIONS

We have constructed a simple occultation model to investigate whether the change in spectral and timing properties between simple and complex NLS1s can be explained by a difference in inclination with respect to a failed wind. In this scenario, clumps of material lifted from the inner parts of the accretion disc by radiation pressure, obscure the X-ray emission for sources seen at high inclination angles, resulting in more extreme variability and more complex spectra. Associating the deep dips with occultation superimposes absorption features from Fe Kα on the dip spectra. This is seen in complex NLS1s such as Mrk 776 (Miller et al. 2007) and is a smoking gun for the reality of these occultation events.

We model the obscuration as a series of individual clouds of constant ionization parameter which transit the inner accretion flow, corotating with the flow and obscure the underlying emission. The underlying accretion flow emission is radially stratified, with the softest X-rays (disc) from the largest radii, and then the soft X-ray excess and corona at progressively smaller radii. We find that occultations add power to the X-ray light curves over a range of frequencies related to the transit time. Occultations also introduce a lag between the hard and soft energy bands when Doppler boosting of the underlying accretion flow emission is taken into account; specifically occultations introduce a soft lead, with the hard band lagging the soft band.

We then combined our occultation model with the full spectral timing model of GD14 which describes the accretion flow emission of the simple NLS1 PG 1244+026. This model also includes reprocessed emission as part of the soft X-ray excess, as well as reflection from it. This reproduces the timing properties of PG 1244+026 by assuming slow fluctuations are generated in the outer components and these propagate down to the corona, producing low-frequency hard lags. The high-frequency soft lags (reverberation lags) are produced predominantly by fast coronal fluctuations being reprocessed in the soft excess wind material rather than by reflection from it.

The effect of the occultations is to dilute the negative reverberation lag and shift it to higher frequencies. By increasing the rate of occultations we can match the change in reverberation lag from the 200 s at 5×10^{-4} Hz seen in the simple NLS1 PG 1244+026 to the $\sim$50 s lag at 10^{-3} Hz seen in the complex NLS1 1H 0707−495. The lag times and light travel times put into the model are the same in both the obscured and unobscured cases. The only difference is the presence of occultations. It is the soft leads caused by the broken symmetry of the ingress and egress of the occultations caused by Doppler boosting of the disc emission which result in a shorter net reverberation lag in the obscured case. The occultations also change the energy spectrum from a simple NLS1, with strong soft excess and a steep power law above 2 keV, to something resembling a complex NLS1, with a prominent iron line from reflection off the soft excess, highly ionized Fe Kα absorption lines and strong spectral curvature.

The short $\sim$50 s reverberation lags have been taken as evidence for extreme relativistic reflection in complex NLS1s. If 50 s really is a light travel time this requires reflection from the innermost radii of an accretion disc around a highly spinning BH. Our occultation model shows that this need not be the case. A short reverberation lag can be the result of a much longer light travel time, diluted and shifted by the soft leads introduced by occulting clouds. In our model, reflection and reprocessing occur between 6 and $12R_{\rm g}$ and puts no constraints on the spin of the BH. Changing inclination then naturally explains the change from smooth spectra to complex spectra, and long lower frequency reverberation lags to shorter higher frequency reverberation lags in simple and complex NLS1s. Given that NLS1s are high accretion rate sources, it is quite natural to expect that the disc is not flat, that radiation pressure can lift material from the disc which will obscure the central emission for high inclination lines of sight. This is a promising geometry to explore further.

ACKNOWLEDGEMENTS

We thank the anonymous referee for helpful comments. EG acknowledges useful discussions with Will Alston and Matt Middleton. CD acknowledges useful conversations with Giovanni Miniutti. EG acknowledges funding from the UK STFC.

REFERENCES

Alston W. N., Done C., Vaughan S., 2014, MNRAS, 439, 1548
Arévalo P., Uttley P., 2006, MNRAS, 367, 801
Boissay R. et al., 2014, A&A, 567, A44
Chevallier L., Collin S., Dumont A.-M., Czerny B., Mouchet M., Gonçalves A. C., Goosmann R., 2006, A&A, 449, 493
Chiang C.-Y., Fabian A. C., 2011, MNRAS, 414, 2345
Collin S., Kawaguchi T., Peterson B. M., Vestergaard M., 2006, A&A, 456, 75
Crummy J., Fabian A. C., Gallo L., Ross R. R., 2006, MNRAS, 365, 1067
Done C., Jin C., Middleton M., Ward M., 2013, MNRAS, 434, 1955
Dovciak M., Svoboda J., Goosmann R. W., Karas V., Matt G., Sochora V., 2014, preprint (arXiv:1412.8627)
Fabian A. C., Miniutti G., Gallo L., Boller T., Tanaka Y., Vaughan S., Ross R. R., 2004, MNRAS, 353, 1071
Fabian A. C. et al., 2009, Nature, 459, 540
Gallo L. C., 2006, MNRAS, 368, 479
Gallo L. C. et al., 2013, MNRAS, 428, 1191
García J., Dauser T., Reynolds C. S., Kallman T. R., McClintock J. E., Wilms J., Eikmann W., 2013, ApJ, 768, 146
Gardner E., Done C., 2014, MNRAS, 442, 2456 (GD14)
Hagino K., Odaka H., Done C., Gandhi P., Watanabe S., Sako M., Takahashi T., 2015, MNRAS, 446, 663
Inoue H., Matsumoto C., 2003, PASJ, 55, 625
Jiang Y.-F., Stone J. M., Davis S. W., 2014, ApJ, 796, 106
Jin C., Done C., Middleton M., Ward M., 2013, MNRAS, 436, 3173
Kara E., Fabian A. C., Cackett E. M., Miniutti G., Uttley P., 2013, MNRAS, 430, 1408
Kara E., Cackett E. M., Fabian A. C., Reynolds C., Uttley P., 2014, MNRAS, 439, L26
Kollatschny W., Zetzl M., 2013, A&A, 558, A26
Kotov O., Churazov E., Gilfanov M., 2001, MNRAS, 327, 799
Krolik J. H., McKee C. F., Tarter C. B., 1981, ApJ, 249, 422
Leighly K. M., 1999, ApJS, 125, 317
Leighly K. M., Moore J. R., 2004, ApJ, 611, 107

Lohfink A. M., Reynolds C. S., Miller J. M., Brenneman L. W., Mushotzky R. F., Nowak M. A., Fabian A. C., 2012, ApJ, 758, 67
Marconi A., Axon D. J., Maiolino R., Nagao T., Pastorini G., Pietrini P., Robinson A., Torricelli G., 2008, ApJ, 678, 693
Matt G. et al., 2014, MNRAS, 439, 3016
Mehdipour M. et al., 2011, A&A, 534, A39
Middleton M., Ingram A., 2015, MNRAS, 446, 1312
Miller L., Turner T. J., 2013, ApJ, 773, L5
Miller L., Turner T. J., Reeves J. N., George I. M., Kraemer S. B., Wingert B., 2007, A&A, 463, 131
Miller L., Turner T. J., Reeves J. N., 2008, A&A, 483, 437
Miller L., Turner T. J., Reeves J. N., Braito V., 2010, MNRAS, 408, 1928
Miniutti G., Fabian A. C., 2004, MNRAS, 349, 1435
Miniutti G., Agís González B., Sanfrutos Carreras M., 2014, in Ness J.-U., ed., The X-ray Universe 2014. Online at http://xmm.esac.esa.int/external/xmm_science/workshops/2014symposium/, id. 141
Miyakawa T., Ebisawa K., Inoue H., 2012, PASJ, 64, 140
Miyamoto S., Kitamoto S., Mitsuda K., Dotani T., 1988, Nature, 336, 450
Nayakshin S., Kallman T. R., 2001, ApJ, 546, 406
Nikołajuk M., Czerny B., Gurynowicz P., 2009, MNRAS, 394, 2141
Nowak M. A., Vaughan B. A., Wilms J., Dove J. B., Begelman M. C., 1999, ApJ, 510, 874
Pancoast A., Brewer B. J., Treu T., 2014, MNRAS, 445, 3055
Patrick A. R., Reeves J. N., Lobban A. P., Porquet D., Markowitz A. G., 2011, MNRAS, 416, 2725
Petrucci P.-O. et al., 2013, A&A, 549, A73
Ponti G. et al., 2010, MNRAS, 406, 2591
Ross R. R., Fabian A. C., 2005, MNRAS, 358, 211
Takeuchi S., Ohsuga K., Mineshige S., 2014, PASJ, 66, 48
Torii S. et al., 2011, PASJ, 63, S771
Turner T. J., Miller L., Reeves J. N., Kraemer S. B., 2007, A&A, 475, 121
Uttley P., Cackett E. M., Fabian A. C., Kara E., Wilkins D. R., 2014, A&AR, 22, 72
Zoghbi A., Uttley P., Fabian A. C., 2011, MNRAS, 412, 59

This paper has been typeset from a TEX/LATEX file prepared by the author.